Materials & Design 213 (2022) 110306

Contents lists available at ScienceDirect

Materials & Design

journal homepage: www.elsevier.com/locate/matdes

Effect of crystal orientation on the hardness and strength of piezoelectric $LiNbO_3$ substrates for microelectronic applications

M. Gruber *, A. Leitner, D. Kiener, P. Supancic, R. Bermejo

Department of Materials Science, Montanuniversitaet Leoben, Franz Josef Strasse 18, A-8700 Leoben, Austria

HIGHLIGHTS

- Hardness anisotropy associated with crystal orientation governs surface damage morphology in $LiNbO_3$.
- A 20% difference in hardness can double the characteristic strength of $LiNbO_3$.
- Tailored high Young's modulus surface planes of $LiNbO_3$ can significantly increase its characteristic strength.

GRAPHICAL ABSTRACT

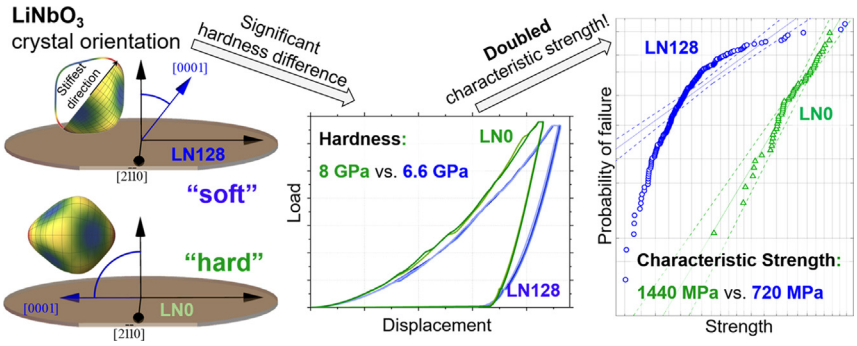

ARTICLE INFO

Article history:
Received 13 July 2021
Revised 3 December 2021
Accepted 6 December 2021
Available online 6 December 2021

Keywords:
Brittle single crystals
Reliability of microelectronic materials
Hardness anisotropy
Strength anisotropy
Biaxial strength
Scratch testing

ABSTRACT

Piezoelectric single crystalline materials are paramount for high-speed data transfer in 5G technologies. The functionality of the end-devices demands temperature independent frequency filtering and high surface acoustic wave velocities, which are associated with the orientation dependent thermo-physical properties of the piezoelectric substrate material. Single crystalline Lithium Niobate ($LiNbO_3$), cut in particular directions, has proven to have outstanding functional properties, yet its brittle character along with the highly anisotropic mechanical properties may limit its use in demanding applications.

In this study, the effect of crystal orientation on hardness and on mechanical strength is demonstrated by comparing nanoindentation results and finite element analysis supported biaxial strength experiments for two $LiNbO_3$ samples with different orientation. It is demonstrated that the crystal anisotropy leads to differences in hardness up to ~ 20% between both orientations, with the characteristic strength being double in the harder direction. The observed correlation is rationalized based on the effect of surface finish and distinct sub-surface damage in the corresponding crystal orientations. Additional strength measurements on nano-scratched samples revealed a significantly higher remaining strength for the harder orientation due to less (sub-) surface damage. These findings can be exploited in future design of single crystalline substrate materials with higher reliability.

1. Introduction

Single crystalline materials have found widespread application in microelectronics due to their outstanding functional properties. In particular, silicon can be considered as the basis of every functional microelectronic system. However, the demand for ever

* Corresponding author at: Chair of Structural and Functional Ceramics, Department of Materials Science, Montanuniversitaet Leoben, Peter-Tunner-Strasse 5, A-8700 Leoben, Austria.

E-mail addresses: manuel.gruber@unileoben.ac.at (M. Gruber), alexander.leitner@rhimagnesita.com (A. Leitner), daniel.kiener@unileoben.ac.at (D. Kiener), peter.supancic@unileoben.ac.at (P. Supancic), raul.bermejo@unileoben.ac.at (R. Bermejo).

https://doi.org/10.1016/j.matdes.2021.110306
0264-1275/

higher packing densities and functionalities makes it necessary to explore the use of other brittle single crystals to be employed as substrates for functional components. An example are single crystalline piezoelectric substrate materials for wave filters, utilized in the 5G technology for mobile devices [1,2]. Two representatives of such materials are $LiTaO_3$ and $LiNbO_3$, which show well-balanced properties in terms of high electromechanical coupling factor, low insertion/propagation loss, low temperature dependences and producibility of sufficiently large diameters at acceptable costs.

The key task of a frequency filter is to allow a certain centre frequency within a bandwidth to pass and simultaneously suppress all other frequencies. For higher frequencies (in the GHz regime), bulk acoustic wave filters (BAWs) may be used [3]. An alternative to such rather expensive technology may be the use of surface acoustic wave (SAW) counterparts, which are in general conceived for lower frequencies, where lithographic as well as wafer bonding techniques originating from the semiconductor industry have been successfully established [1,4–7]. Therefore, a further development targets to expand the application range of SAWs by shifting the filtered centre frequency to higher values. This can be achieved by reducing the electrode's width and/or spacing between electrodes, were the geometric limits are associated with the lithographic process. Another possibility is to increase the wave velocity of the substrate, which is proportional to the centre frequency. In such case, both the chosen substrate material itself and the corresponding orientation (in case of single crystals) can strongly influence this property. For instance, in certain orientation, $LiNbO_3$ has been found to provide extraordinarily high wave velocities as high as $\sim$ 4000 m/s, making it exceptionally suitable for SAW substrates [8,9].

Despite the use of piezoelectric crystals for their functional properties, structural integrity of the substrate material during in-service conditions must be preserved. Since in a microelectronic system different material classes (polymers, metals, ceramics) with distinct thermo-mechanical properties are combined, this may compromise the mechanical reliability of the component when they are exposed to significant changes in temperature (e.g. during production or in service) [10–13]. In case such stresses overcome the component strength, cracks may arise and the functionality of the entire microelectronic system may be no longer guaranteed. As such, it would be of importance to identify crystallographic orientations that not only provide high wave velocities, but at the same time also increase the mechanical robustness by limiting the tendency to fracture and increase the characteristic material strength to avoid overload failure.

Previous studies have revealed a strong dependence of the strength of piezoelectric crystals, such as $LiTaO_3$ and $LiNbO_3$, on the orientation with respect to the loading plane [14]. In addition, a significant effect of the surface condition (i.e., mirror-polished, grinded, or nano-scratched) on the strength distribution could be observed and quantified [15]. Furthermore, it was found that $LiTaO_3$ and $LiNbO_3$ materials displayed significant difference in hardness, which may result in different surface (or sub-surface) defect populations associated with the polishing process [16]. In this regard, low biaxial strength values (compared to chemically similar $LiTaO_3$ single crystals) together with non-Weibullian strength distributions were measured for a particular orientation in $LiNbO_3$ material [14]. In that case, the surface corresponds to the $(0\ \bar{1}\ 14)$ crystallographic plane, which is known to have relatively low hardness [17].

To the best of our knowledge, it is currently unclear whether a direct correlation exists between strength, hardness and orientation in piezoelectric brittle crystals such as $LiNbO_3$. It is hypothesized that hardness anisotropy, as observed for many single crystalline materials [18–20], may have an effect on the defect formation during polishing, thus influencing the strength distribution of the material and corresponding reliability of the substrate, but detailed knowledge is lacking.

Therefore, the aim of this work is to quantify the effect of crystal orientation on hardness and subsequently strength distribution in $LiNbO_3$ piezoelectric materials. Two different crystallographic orientations are chosen for the investigation. Hardness and indentation equivalent elastic modulus of the two differently oriented samples are measured using nanoindentation. Furthermore, a miniaturized biaxial bending test, the ball-on-three-balls (B3B) testing method, is employed in combination with finite element analysis (FEA) to account for anisotropy effects on failure stress determination. The thereby derived Weibull evaluation accounting for anisotropy is employed in order to compare the strength of the two orientations. To gain a deeper insight into the damage behaviour responsible for pre-existing surface defects, besides common post-mortem fractography, controlled scratch experiments using a Berkovich nanoindenter tip are performed on both orientations, followed by biaxial bending tests on these pre-damaged samples to relate the fracture characteristics to a well-defined initial defect. These controlled experiments shed a light on the influence of surface treatments with respect to resulting characteristic strengths and will enable optimized polishing procedures in the future.

2. Materials and methods

2.1. Materials & wafer surface:

As a non-centrosymmetric material, $LiNbO_3$ shows various functional properties of great interest such as pyro-electricity, non-linear optical behaviour or piezo-electricity [21], which may be exploited best when the material is used in single crystalline form. It has a trigonal crystal structure which may be translated into a more convenient hexagonal one (as done in this work). Corresponding parameters of the unit cell are: $a_h = b_h = 5.148$ Å and $c_h = 13.863$ Å [22]. Like other single crystalline materials, $LiNbO_3$ shows orientation dependent functional as well as mechanical properties, where the latter ones are of interest in this work. In this context, the orientation dependent Young's modulus (at a constant electric field) is plotted in Fig. 1 according to the values obtained

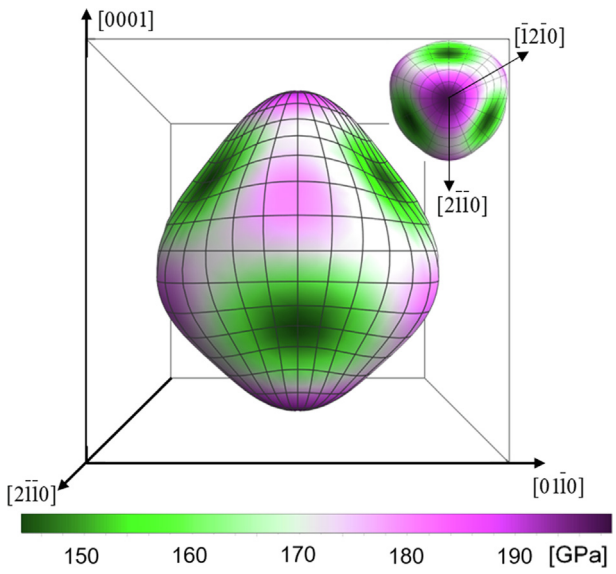

Fig. 1. Orientation dependent Young's modulus of $LiNbO_3$ at constant electric field. The highest values are evident along the [0001] direction.

from Smith et al. [23]. It can be seen that the highest values are observed along the hexagonal c-axis, corresponding to the [0001] direction, which therefore represents the direction with the strongest chemical bonds.

According to the application the single crystalline material has been conceived for, a certain wafer orientation is usually preferable. For the application as SAW filter, an angle of 128° between the wafer surface and the c-axis ("LN128") is often chosen due to the high wave velocity of this cut together with low insertion loss and acceptable temperature coefficients [8,9]. This cut corresponds to a rotation of ~ 38° of the c-axis around the x-axis towards the y-axis (see Fig. 2a). The direction dependent Young's modulus is rotated in the same way and also indicated in Fig. 2a). For this cut, where the strong bonds along the c-axis are far away from being in the surface plane or perpendicular to it, the relatively soft $(0\ \bar{1}\ 14)$ plane is parallel to the surface.

As far as hardness is concerned, the orientation dependent value may be predictable for many materials based on the electronegativity [24]. Unfortunately, such an approach is not suitable for materials containing highly ionic bonds, such as $LiNbO_3$. However, hardness is determined by the elastic bulk and shear modulus [25], which are, together with Poisson's ratio, of great relevance for design tasks [26]. For $LiNbO_3$ it can be summarized that the strongest atomic bonds are aligned along the [0001] direction (see Fig. 1). It is hypothesized that rotating the strong bonds in plane may increase the hardness of the material. This orientation, with the [0001] direction being parallel to the surface plane ("LN0"), is illustrated in Fig. 2b). Thereby, the surface corresponds to the $(01\ \bar{1}\ 0)$ plane.

For both orientations (LN128 and LN0, see Fig. 2a and b), specimens for biaxial bending (B3B-experiments) were manufactured from mirror polished 4″ wafers with dimensions of 2 × 2 mm^2, with corresponding wafer thickness of 0.133 mm for LN128 and 0.140 mm for LN0, respectively.

The mirror polished surfaces were investigated on a VK-X1000 confocal microscope (Keyence, Osaka, Japan). Average roughness values of S_a = 1–2 nm were measured on representative areas (~210 × 280 μm), as shown in Fig. 2. The highest and lowest points on the investigated areas differ by around 10–12 nm for both materials. For LN128 (Fig. 2a) a streaky surface pattern repeating every ~ 30 μm is observed, whereas for LN0 (Fig. 2b) a chequerboard pattern with similar peak distances (~15–30 μm) was detected. It is worth mentioning that regarding possible effects on the strength, no significant differences in roughness and morphology could be observed.

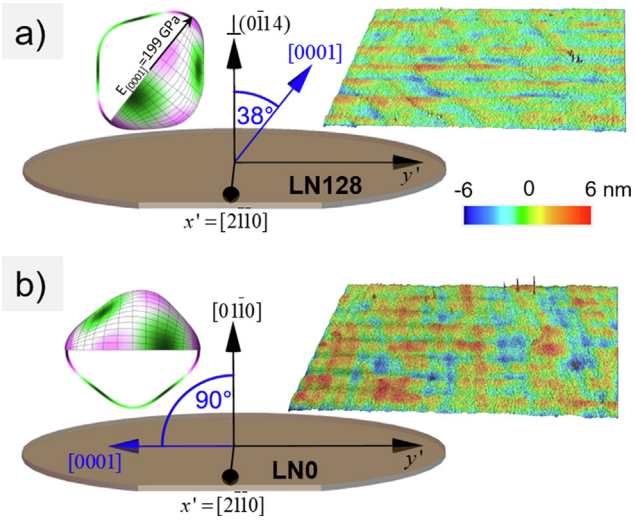

Fig. 2. (a) Orientation of the strongest atomic bonds for "soft" surface ("LN128") and (b) for "hard" surface ("LN0") together with 3D confocal microscope images of the respective surfaces. No significant differences in morphology and roughness possibly affecting the strength are evident.

2.2. Nanoindentation & nanoscratch

Nanoindentation experiments have been performed on LN128 and LN0, respectively, in order to retrieve hardness as well as indentation equivalent elastic modulus for both orientations of the single crystalline $LiNbO_3$ material. All indentation experiments were carried out on a G200 nanoindenter (Keysight-Tec, Santa Rosa, California, USA) equipped with a diamond Berkovich tip (Synton-MDP AG, Nidau, Switzerland) and using a continuous stiffness measurement (CSM) unit. Calibration experiments were conducted on fused silica. Constant strain rates of$\dot{P}/P$ = 0.05 s^{-1} and a displacement amplitude of 2 nm at a frequency of 45 Hz for the CSM signal were chosen for the conducted displacement-controlled experiments. For this setting no influences of the integrated lock-in amplifier are to be expected [27]. The same applies for thermal drift, which was measured in a post-test segment, where it did not exceed 0.3 nm/s for any indent performed. For both orientations, hardness as well as indentation equivalent modulus, were determined according to Oliver and Pharr [28], with the latter value being calculated from the received reduced modulus during indentation and the materials Poisson's ratio (ν = 0.25) together with elastic constants for the tip (E = 1141 GPa, ν = 0.07 [29]). Correction of the obtained values according to Vlassak and Nix to account for anisotropic materials behaviour were neglected due to the low anisotropy factor of 1.4 (calculated using data from [23]), since the maximum possible influence should be below 2% [30,31] and thus well within the overall measurement uncertainties.

For the scratched samples, the same nanoindenter equipped with a Berkovich tip was utilized to perform scratches in the centre of the specimen, parallel to one of the most critical $\{01\ \bar{1}\ 2\}$ cleavage planes [32] and with the indenter edge ahead for both crystal orientations. Scratch load, speed and length were set to 10 mN, 1 μm/s and 100 μm, respectively.

2.3. Biaxial strength testing methods and finite element analysis

For the strength measurements conducted in this work, a biaxial testing method, the B3B test [33,34], schematically illustrated in Fig. 3a, was employed in order to account for the expected anisotropic fracture behaviour of the single crystalline materials. Further advantages of this test are that only the surface of the specimen is exposed to the highest tensile stress (no influence of edge defects), and the possibility to test specimens with dimensions close to a final SAW-device (side lengths in the mm-regime and thickness of ~ 100–200 μm) [4,35]. The specimens with dimensions of 2 × 2 × 0.133 mm^3 for LN128 and 2 × 2 × 0.140 mm^3 for LN0 were marked with coloured dots in the corners before extracting to ensure traceability of the crystallographic orientation, indicated in Fig. 3b and c bottom right with respect to the orientation indicated in Fig. 2. For the subsequent B3B test the specimen was supported by three balls and loaded through a fourth ball (diameter of ~ 1.19 mm for all four balls) on the opposite side (see Fig. 3a), leading to a well-defined biaxial stress field on the opposite side of the loading ball.

Pre-loads between 0.5 and 2 N were chosen to guarantee contact between the specimen and the four balls prior testing. A cross-head displacement speed of 0.1 mm/min was employed up to the fracture load on a universal testing machine (Zwick Z010,

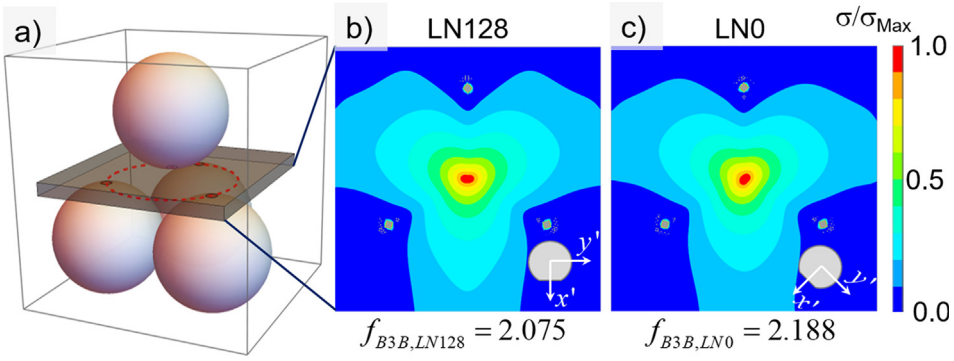

Fig. 3. (a) Schematic representation of the conducted B3B test; (b) stress field and f-factor for the LN128 orientation and (c) stress field and f-factor for the LN0 configuration.

Zwick/Roell, Ulm, Germany). For the LN128 sample without scratches, data pooling with already published results was performed. Thereby, samples with testing speeds of 0.01–1 mm/min tested in water and air have been combined since no significant sub-critical cack growth phenomena could be measured in the respective previous work [14] and were recalculated taking into account the anisotropic elastic behaviour, as considered in this work. The stress distribution in the $LiNbO_3$ specimens (see Fig. 3b and Fig. 3c for LN128 and LN0, respectively) has thereby been calculated with the commercial FEM-package ANSYS Release 2021R2 within a linear elastic approach with values taken from [23]. About 400,000 2nd order brick elements (SOLID186) corresponding to about 1.5 million nodes were used to setup the FE model for the full specimen (note: the full model is necessary due to the lack of symmetry). The anisotropy of the material has been fully accounted, as well as the two special orientations of the crystals (LN128, LN0) in the B3B-loading condition. The supports of the three balls were idealized by displacement constraints on the corresponding nodes, while the load was modelled by a central force perpendicular to the surface. The stress maximum occurs on the tensile loaded side nearly opposite to the central force position, but due to the non-symmetric general orientation of the elastic material tensor the maximum position is slightly off centre in the plate.

The corresponding failure stress (σ_f) was calculated out of the maximum load (P) after the B3B test according to:

$$\sigma_f = f \cdot \frac{P}{t^2} \tag{1}$$

with (t) being the specimen thickness. The factor f retrieved from the finite element simulations has a value of 2.075 for the LN128 (0.133 mm thick) and 2.188 for the LN0 (0.140 mm thick) specimens, respectively. Failure stress values were interpreted within the Weibull theory [36] following the recommendations as given in EN 843-5 standard [37]. For the scratched tests 15 specimens per sample were prepared and tested.

3. Results & discussion

3.1. Nanoindentation

Fig. 4 shows representative load–displacement curves for the two differently oriented $LiNbO_3$ specimens. The flatter curve belongs thereby to LN128 (reproduced using data from [16]) and the steeper one to LN0. Correspondingly, the obtained values for hardness and indentation equivalent elastic modulus are higher for the latter one and can be obtained from the table inserted in Fig. 4. Especially the hardness of LN0 is with 8.0 GPa ~ 21% higher compared to the previously published value of LN128 (6.6 GPa),

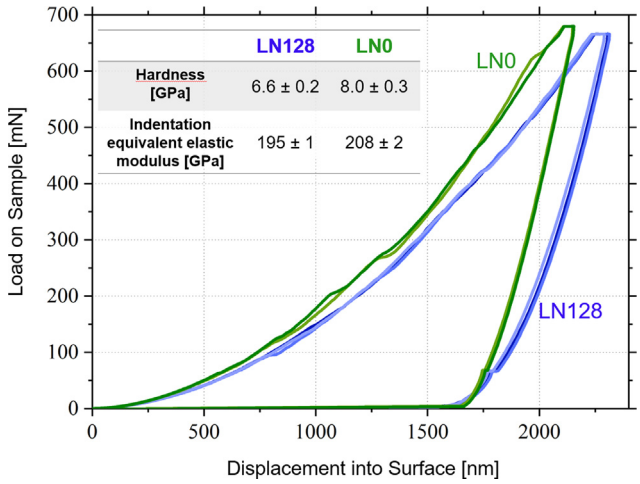

Fig. 4. Representative load vs. displacement curves for LN128 (blue, reproduced data from [16]) and LN0 (green) with inserted table containing corresponding hardness and indentation equivalent elastic modulus values. The measured hardness of LN0 is ~ 20% higher compared to the LN128 orientation.

while for the indentation equivalent elastic modulus only a slight increase of ~ 7% was observed for LN0 (208 GPa) compared to LN128 (195 GPa), with data for LN128 being taken from [16]. Hardness values are within the expected range for $LiNbO_3$ as summarized in [38]. The same applies for indentation equivalent elastic modulus as reported for different wafer cuts in [39]. As far as anisotropy is concerned, it is noteworthy pointing out that Csanadi et al. reported similar relative differences in ZrO_2 when the hardest and stiffest orientation was compared with the softest and most compliant one [40].

3.2. Strength evaluation

The strength distributions for the two samples are represented in a Weibull diagram (see Fig. 5) where values for LN128 were taken from previous work [14], but recalculated taking the f-factor for the elastically anisotropic case (see details in section 2.3). The probability of failure (F) is plotted versus the failure stress (σ), where the latter one is being calculated according to Eq. (1). The corresponding Weibull parameters σ_0 and m (characteristic strength and Weibull modulus, respectively) were evaluated using the EN-843–5 standard [37].

It can be summarized that the characteristic strength of the sample with the harder surface (LN0), i.e. σ_0 = 1442 [1396–1489] MPa is twice the characteristic strength of the sample with softer surface (LN128), i.e. σ_0 = 724 [693–757] MPa. These findings are

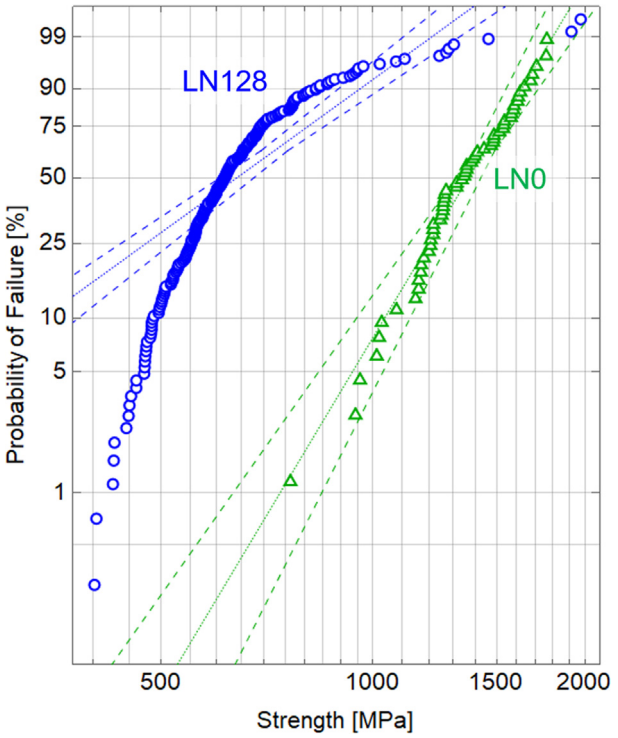

Fig. 5. Weibull diagram for LN128 (blue circles, recalculated data from [14] taking into account the anistropic elastic material behaviour according to chapter 2.3) and LN0 (green triangles). The dotted line represents the Weibull fit, the dashed lines the corresponding 90% confidence intervals.

in contrast to plastically deformable materials such as metals, where a linear relationship between strength and hardness is generally reported [41,42]. However, for brittle materials such as $LiNbO_3$, which fail before reaching their yield strength, no such general relationship has been observed [41]. For these materials, the strength is determined by the combination of defect (size) and fracture toughness, where the latter one does not vary significantly for brittle engineering materials [42]. Nevertheless, hardness represents the resistance of a material against penetration of foreign bodies and can therefore significantly influence the mechanical reliability: In this regard, surface defects originating from production (grinding, polishing) or service are usually identified as the main cause of failure. Such fracture behaviour may be also expected for single crystals, where no large volume defects are present.

The LN0 distribution seems to follow a Weibullian behaviour with $m \sim 7$, which is relatively high for a mirror polished single crystalline material where usually m values of 3–5 are reported [35,43,44]. In comparison, LN128 is strongly deviating from a two parameter Weibull distribution and can neither be described with a three-parameter distribution. An explanation to this finding may be provided by the work of Danzer et. al [45], where the influence of different artificial flaw distributions is discussed. For a distribution with an extraordinarily high density of defects within a certain size range, a similar "banana" shaped curve may be obtained when the tested effective volume is within a certain range. Such behaviour may be the consequence of a grinding and/or polishing step, where damage is caused by a certain size of the particles in the abrasive medium. This could cause a high density of flaws within a small size range, which could explain the strong deviation from Weibullian behaviour for the softer sample. For the harder surfaces, however, this damage may not be severe enough and may be removed in following polishing steps due do the higher resistance against penetration of foreign bodies, resulting in the observed Weibull behaviour of LN0.

3.3. Fractography

Examination of fracture surfaces on brittle materials can reveal important information on the type, shape and location of the critical defect in the specimen. In case of single crystalline materials, which hold a high strength and therefore feature small flaw sizes, specimens are typically fractured into a large number of fragments. This fact in combination with the already small specimen size made examinations of pristine specimens challenging. In order to overcome this issue, selected specimens were mounted on an adhesive tape and then loaded to failure in the same B3B configuration. Fragments were kept together by the tape and could be analysed post-mortem. Representative specimens are shown in Fig. 6 for LN128 (left) and LN0 (right) together with schematically reconstructed fracture patterns underneath. The thinner the line, the steeper is the angle to the surface and the more critical the plane is aligned for cleavage in the applied testing method. This correlation is plotted in the supplementary figure for a thickness of 0.133 mm. For LN128, the $(0\ 1\ \bar{1}\ 2)$ and $(1\ 0\ \bar{1}\ 1)$ planes are almost perpendicular to the surface and were clearly activated (see Fig. 6, left). The crack along $(1\ 0\ \bar{1}\ 1)$ turns into the $(1\ \bar{1}\ 0\ 0)$ plane at some distance to the centre. For LN0, the most critical cleavage planes are $(1\ \bar{1}\ 0\ 2)$ and $(\bar{1}\ 0\ 1\ 2)$, with an angle of $\sim 65°$ to the surface, and were visible on every specimen (see Fig. 6, right). Interestingly, also $(01\ \bar{1}\ 2)$ with an angle of only $\sim 33°$ was activated regularly. The same applies for the $(\bar{1}\ \bar{1}\ 23)$ and $(1\ \bar{2}\ 13)$ planes, both with an angle of $\sim 41°$ to the surface. The $(\bar{2}\ 16)$ and $(2\ \bar{1}\ 6)$ cleavage planes identified by Hirsh et al. [46] would lead to similar surface fracture patterns. However, for the LN0 orientation they are both perpendicular to the surface, which does not fit to the actual crack path observed in this work.

Due to the many fragments, SEM investigations could not reveal the fracture origin and primary crack. It can only be speculated that the facture origin may be a scratch acting as a surface defect, aligned parallel to a critical cleavage plane, as observed in previous work [15].

3.4. Scratch tests and strength evaluation

For a deeper understanding of the indirectly measured surface damage behaviour of LN128 and LN0, scratch experiments with a diamond Berkovich tip were conducted. This may give detailed insights into possible mechanisms occurring when a relative movement between hard particles (e.g. from the abrasive medium) and the sensitive wafer surface occurs. Fig. 7 shows the displacement into surface vs. scratch distance plots for LN128 (reproduced data from [15]) and LN0, respectively. Both scratching directions were parallel to a $\{01\ \bar{1}\ 2\}$ cleavage plane with the steepest angle to the surface (e.g. the most critical cleavage plane for the respective orientation in combination with B3B testing). It can be seen that the mean displacement depth for LN0 is slightly lower while showing higher scatter compared to LN128. The lower penetration depth can be related to the higher hardness and Young's modulus of LN0. The reason for the higher scatter, however, is only visible in the SEM images inserted in Fig. 7 for both materials. While for LN128 a very continuous and smooth scratch remains at the surface, a stepped morphology appears for LN0. Further, for LN128 a continuous open crack (marked with blue arrows) seems to open (cross sections may be retrieved from [15]) while for LN0 flaking off seems to be the main damage mechanism for this scratch orien-

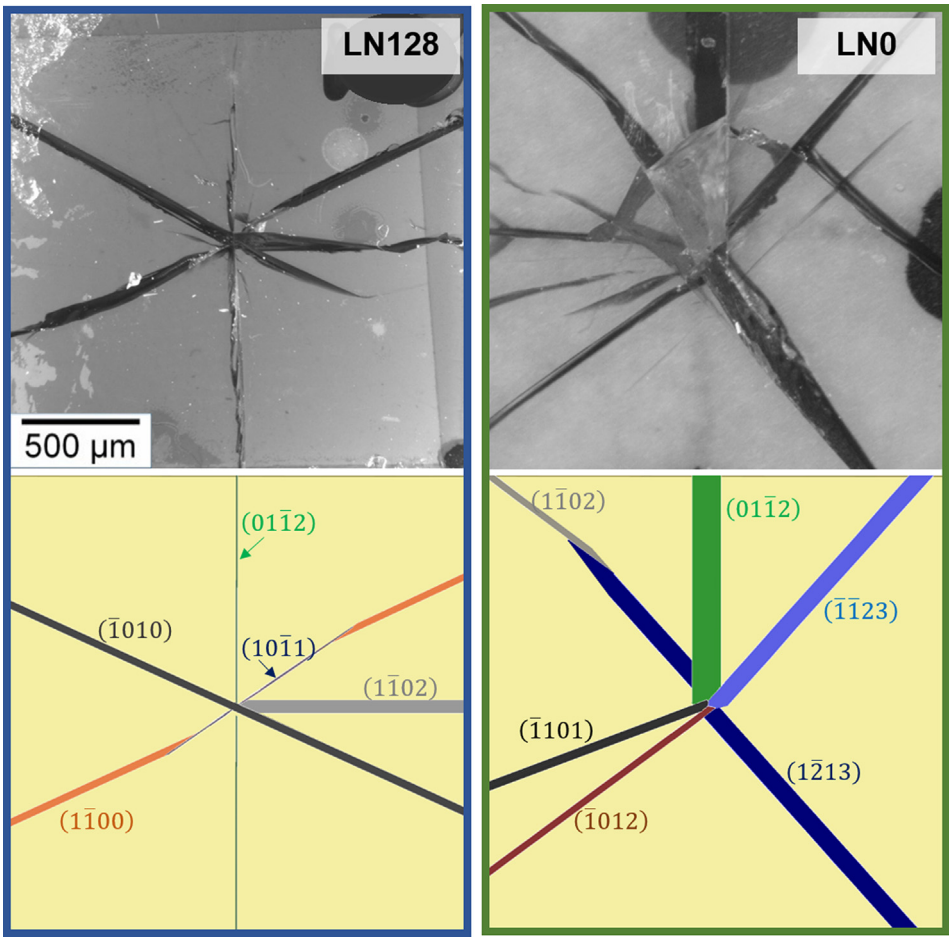

Fig. 6. Representative fracture patterns of LN128 and LN0, respectively, together with reconstruction of the pattern using certain crystallographic planes. Thin lines or cracks, respectively, indicate a steeper angle to the surface of the corresponding crystallographic plane.

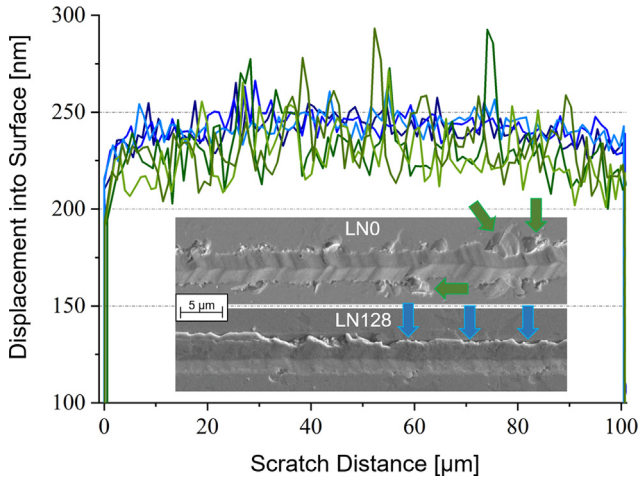

Fig. 7. Displacement into surface vs. scratch distance for LN128 (blue, reproduced data from [15]) and LN0 (green) with representative surfaces inserted below. For LN128 a continuous crack (blue arrows) seems to open, while for LN0 flaking off of material (green arrows) seem to be the dominant damage mechanism. (For interpretation of the references to colour in this figure legend, the reader is referred to the web version of this article.)

tation (highlighted with green arrows in Fig. 7). As far as subsurface damage is concerned, also a non-continuous damage mechanism as described in [47] may be expected for the LN0 configuration accordingly.

For $LiNbO_3$ it is already known that the scratch orientation may strongly affect the damage morphology in terms of onset, severity and direction of cracking and chipping together with strong differences in brittle to ductile transition depth/load [39]. Nevertheless, for both orientations, the scratch is parallel to the most critical {01 $\bar{1}$ 2} cleavage plane, which is expected to cause the highest loss in strength.

In order to evaluate the effect of the artificial surface damage on the strength, biaxial strength measurements (B3B tests) of the scratched specimens were performed for LN0 and compared to previous results. Fig. 8 shows the Weibull diagram for LN0 from this work together with recalculated data from [15] taking into account the elastic anisotropy as described in section 2.3. Both show a strong decrease in strength compared to their not pre-damaged counterparts (see. Fig. 5 for comparison) by a factor of $\sim$ 2.6–2.8. Thus, the remaining strength for the pre-damaged LN0 (520 [452 – 601 MPa]) is higher by a factor of 1.8 compared to pre-damaged LN128 (282 [255 – 314 MPa]), even though for both orientations scratches were made parallel to the most critical {01 $\bar{1}$ 2} cleavage plane for this testing configuration. In light of these findings it can be claimed that for the same, very defined and reproducible introduction of artificial surface damage, the corresponding size of these defects is smaller for the harder orientation (see Fig. 8 bottom right). Corresponding effective defect sizes were thereby estimated (assuming linear elastic fracture behaviour) according to:

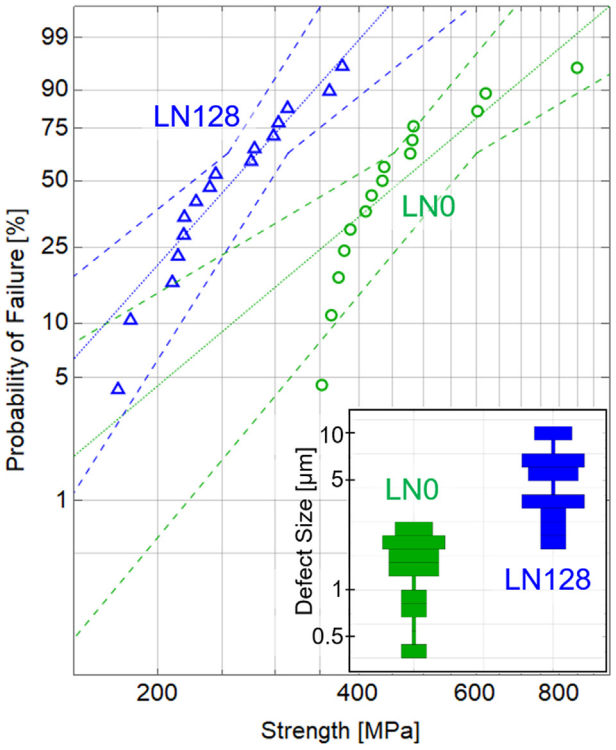

Fig. 8. Weibull diagram for scratched LN128 (blue triangles, recalculated from [15] respecting the anisotropic elastic behaviour according to chapter 2.3) and LN0 (green circles) samples. The dotted line represents the Weibull fit, the dashed lines the corresponding 90% confidence intervals. A significantly higher remaining strength is evident for the harder LN0 sample after introducing artificial scratches. Estimated effective defect sizes are provided in the insert bottom right. (For interpretation of the references to colour in this figure legend, the reader is referred to the web version of this article.)

$$a_c = \frac{1}{\pi}\left(\frac{K_{IC}}{Y\sigma}\right)^2 \quad (2)$$

with Y = 1.12 [48] for a surface scratch and K_{IC} = 1.1 [32] for $LiNbO_3$.

In summary, the example of $LiNbO_3$ has evidenced the strong dependence of crystal orientation on the mechanical reliability of SAW filters, which are indispensable components in the modern communication market. Even though the functional properties may not be sufficient for their use as "bulk" substrate, new technologies combining the piezo substrate with quartz glass [49] or multilayer approaches [50] may open the way for utilizing new crystal orientations with enhanced functional properties and structural integrity. The utilization of combined nanoindentation techniques with biaxial strength measurements and fractography has proven successful to understand the effect of damage behaviour and mechanical reliability in differently oriented $LiNbO_3$ wafers, and may be recommended for reliability analysis in other single crystalline materials.

4. Conclusion

This work analysed a reference material used in SAW applications, $LiNbO_3$, with mirror polished surface and two different crystallographic orientations to demonstrate the strong effect of hardness anisotropy in single crystalline materials and the relation to mechanical strength.

Nanoindentation measurements revealed an increase in hardness of ~ 20% when the strongest atomic bonds are aligned parallel to the indented surface. This slight increase in hardness, however, doubles the measured biaxial bending strength. Artificial flaws introduced through scratch experiments revealed a difference in damage morphology correlating to the orientation dependent hardness. The harder $LiNbO_3$ sample exhibited a much higher remaining strength, which could be ascribed to the different damage patterns observed. These patterns, on the other hand, depend on the combination of crystallographic orientation of the surface and scratch direction. While for the softer LN128 cracks into the depth seem to open, flaking-off of surface material is the dominant damage mechanism for the harder LN0, resulting in overall lower average penetration depth of the indenter tip for the same applied load.

As generalized conclusion, the surface conditioning of brittle (single crystalline) materials can strongly influence the strength of the substrate material and therefore the mechanical reliability of the end component due to a crystallographic orientation dependent hardness.

Declaration of Competing Interest

The authors declare that they have no known competing financial interests or personal relationships that could have appeared to influence the work reported in this paper.

References

[1] D. Morgan, Surface Acoustic Wave Filters, 2nd ed., Academic Press, 2007.
[2] S. Mahon, The 5G Effect on RF Filter Technologies, IEEE Trans. Semicond. Manuf. 30 (4) (2017) 494–499, https://doi.org/10.1109/TSM.2017.2757879.
[3] K.-Y. Hashimoto, RF Bulk Acoustic Wave Filters for Communications, ARTECH HOUSE (2009).
[4] T. Bauer, C. Eggs, K. Wagner, P. Hagn, A Bright Outlook for Acoustic Filtering: A New Generation of Very Low-Profile SAW, TC SAW, and BAW Devices for Module Integration, IEEE Microwave Magaz. 16 (7) (2015) 73–81.
[5] B. Hu, S. Zhang, H. Zhang, W. Lv, C. Zhang, X. Lv, H. San, Fabrications of L-Band $LiNbO_3$-Based SAW Resonators for Aerospace Applications, Micromachines. 10 (6) (2019) 349, https://doi.org/10.3390/mi10060349.
[6] J. Chao, D. Liu, S. Chiu, C.S. Chang, H. Ru, Ultra-miniature SAW filter new structure: for 5G IoT mobile device, in: 2019 14th International Microsystems, Packaging, Assembly and Circuits Technology Conference (IMPACT). (2019) 51-53. https://doi.org/10.1109/IMPACT47228.2019.9024957.
[7] R. Takigawa, J. Utsumi, Direct bonding of $LiNbO_3$ and SiC wafers at room temperature, Scripta Mater. 174 (2020) 58–61, https://doi.org/10.1016/j.scriptamat.2019.08.027.
[8] K. Shibayama, K. Yamanouchi, H. Sato, T. Meguro, Optimum Cut for RoV-Cut LiNb03 Crystal Used as the Substrate of Acoustic-Surface-Wave Filters, Proc. IEEE 64 (1976) 595–597, https://doi.org/10.1109/PROC.1976.10181.
[9] C. Campbell, Surface Acoustic Wave Devices and their Signal Processing Applications, Academic Press (1989) 427–458.
[10] C.H. Hsueh, A.G. Evans, Residual Stresses and Cracking in Metal/Ceramic Systems for Microelectronics Packaging, J. Am. Ceram. Soc. 68 (3) (1985) 120–127, https://doi.org/10.1111/j.1151-2916.1985.tb09648.x.
[11] M. Gruber, P. Supancic, F. Aldrian, R. Bermejo, Effect of metallization on the strength and fracture behaviour of functional co-fired multilayer ceramics, J. Eur. Ceram. Soc. 37 (14) (2017) 4389–4396, https://doi.org/10.1016/j.jeurceramsoc.2017.02.018.
[12] P. Lall, M.G. Pecht, E.B. Hakim, Influence of Tempemture on Microelectronics and System Reliability: A Physics of Failure Approach, CRC Press, 2020.
[13] M. Gruber, I. Kraleva, P. Supancic, R. Danzer, R. Bermejo, A novel approach to assess the mechanical reliability of thin, ceramic-based multilayer architectures, J. Eur. Ceram. Soc. 40 (14) (2020) 4727–4736, https://doi.org/10.1016/j.jeurceramsoc.2020.02.016.
[14] M. Gruber, I. Kraleva, P. Supancic, J. Bielen, D. Kiener, R. Bermejo, Strength distribution and fracture analyses of $LiNbO_3$ and $LiTaO_3$ single crystals under biaxial loading, J. Eur. Ceram. Soc. 37 (14) (2017) 4397–4406, https://doi.org/10.1016/j.jeurceramsoc.2017.02.002.
[15] M. Gruber, A. Leitner, I. Kraleva, D. Kiener, P. Supancic, R. Bermejo, Understanding the effect of surface flaws on the strength distribution of brittle single crystals, J. Am. Ceram. Soc. 101 (12) (2018) 5705–5716.
[16] M. Gruber, A. Leitner, D. Kiener, P. Supancic, R. Bermejo, Incipient plasticity and surface damage in $LiTaO_3$ and $LiNbO_3$ single crystals, Mater. Des. 153 (2018) 221–231, https://doi.org/10.1016/j.matdes.2018.04.082.
[17] S. Bhagavat, I. Kao, Nanoindentation of lithium niobate: hardness anisotropy and pop-in phenomenon, Mater. Sci. Eng., A 393 (1-2) (2005) 327–331, https://doi.org/10.1016/j.msea.2004.11.027.
[18] C. Brookes, J. O'neill, B. Redfern, Anisotropy in the hardness of single crystals, Proc. Royal Soc. London. A. Math. Phys. Sci. 322 (1971) 73-88. https://doi.org/10.1098/rspa.1971.0055.

[19] F. Ebrahimi, L. Kalwani, Fracture anisotropy in silicon single crystal, Mater. Sci. Eng., A 268 (1-2) (1999) 116–126, https://doi.org/10.1016/S0921-5093(99)00077-5.
[20] K. Eswar Prasad, K.T. Ramesh, Hardness and mechanical anisotropy of hexagonal SiC single crystal polytypes, J. Alloy. Compd. 770 (2019) 158–165, https://doi.org/10.1016/j.jallcom.2018.08.102.
[21] K.K. Wong, Properties of Lithium Niobate, INSPEC, The Institution of Electrical Engineers, London, United Kingdom, 2002.
[22] R. Hsu, E.N. Maslen, D. Du Boulay, N. Ishizawa, Synchroton X-ray Studies of $LiNbO_3$ and $LiTaO_3$, Acta Crystallogr. Sect. B. 53 (1997) 420–428, https://doi.org/10.1107/S010876819600777X.
[23] R.T. Smith, F.S. Welsh, Temperature Dependence of the Elastic, Piezoelectric, and Dielectric Constants of Lithium Tantalate and Lithium Niobate, J. Appl. Phys. 42 (6) (1971) 2219–2230, https://doi.org/10.1063/1.1660528.
[24] K. Li, P. Yang, D. Xue, Anisotropic hardness prediction of crystalline hard materials from the electronegativity, Acta Mater. 60 (1) (2012) 35–42, https://doi.org/10.1016/j.actamat.2011.09.011.
[25] J.J. Gilman, R.W. Cumberland, R.B. Kaner, Design of hard crystals, Int. J. Refract. Met. Hard Mater. 24 (1-2) (2006) 1–5, https://doi.org/10.1016/j.ijrmhm.2005.05.015.
[26] J. Kim, D-i. Cho, R.S. Muller, Why is (111) Silicon a Better Mechanical Material for MEMS? (2001) 662-665. https://doi.org/10.1007/978-3-642-59497-7_157.
[27] B. Merle, V. Maier-Kiener, G.M. Pharr, Influence of modulus-to-hardness ratio and harmonic parameters on continuous stiffness measurement during nanoindentation, Acta Mater. 134 (2017) 167–176, https://doi.org/10.1016/j.actamat.2017.05.036.
[28] W.C. Oliver, G.M. Pharr, An improved technique for determining hardness and elastic modulus using load and displacement sensing indentation experiments, J. Mater. Res. 7 (6) (1992) 1564–1583, https://doi.org/10.1557/JMR.1992.1564.
[29] G. Simmons, H. Wang, Single Crystal Elastic Constants and Calculated Aggregate Properties: A Handbook, 2nd ed., MA, MIT Press, Cambridge, 1971.
[30] J.J. Vlassak, W.D. Nix, Indentation modulus of elastically anisotropic half spaces, Philos. Mag. A 67 (5) (1993) 1045–1056, https://doi.org/10.1080/01418619308224756.
[31] J.J. Vlassak, W.D. Nix, Measuring the elastic properties of anisotropic materials by means of indentation experiments, J. Mech. Phys. Solids. 42 (8) (1994) 1223–1245, https://doi.org/10.1016/0022-5096(94)90033-7.
[32] M. Gruber, R. Konetschnik, M. Popov, J. Spitaler, P. Supancic, D. Kiener, R. Bermejo, Atomistic origins of the differences in anisotropic fracture behaviour of $LiTaO_3$ and $LiNbO_3$ single crystals, Acta Mater. 150 (2018) 373–380, https://doi.org/10.1016/j.actamat.2018.03.020.
[33] A. Börger, P. Supancic, R. Danzer, The ball on three balls test for strength testing of brittle discs: stress distribution in the disc, J. Eur. Ceram. Soc. 22 (9-10) (2002) 1425–1436, https://doi.org/10.1016/S0955-2219(01)00458-7.
[34] R. Danzer, P. Supancic, W. Harrer, Biaxial Tensile Strength Test for Brittle Rectangular Plates, J. Ceram. Soc. Jpn. 114 (1335) (2006) 1054–1060, https://doi.org/10.2109/jcersj.114.1054.
[35] M. Deluca, R. Bermejo, M. Pletz, M. Wießner, P. Supancic, R. Danzer, Influence of deposited metal structures on the failure mechanisms of silicon-based components, J. Eur. Ceram. Soc. 32 (16) (2012) 4371–4380, https://doi.org/10.1016/j.jeurceramsoc.2012.06.027.
[36] W. Weibull, A statistical distribution function of wide applicability, J. Appl. Mech. 18 (1951) 253, https://doi.org/10.1115/1.4010337.
[37] EN 843-5, Advanced Technical Ceramics - Monolithic Ceramics - Mechanical Tests at Room Temperature - Part 5: Statistical Analysis. 1997. p. 40.
[38] K.G. Subhadra, K. Kishan Rao, D.B. Sirdeshmukh, Systematic hardness studies on lithium niobate crystals, Bull. Mater. Sci. 23 (2) (2000) 147–150, https://doi.org/10.1007/BF02706557.
[39] N. Zhu, J. Chen, P. Zhou, Y. Zhu, Effect of the Anisotropy Mechanical Properties on LN Crystals Fixed-Abrasive Lapping, Materials (Basel). 13 (19) (2020) 4455, https://doi.org/10.3390/ma13194455.
[40] T. Csanádi, S. Grasso, A. Kovalčíková, J. Dusza, M. Reece, Nanohardness and elastic anisotropy of ZrB_2 crystals, J. Eur. Ceram. Soc. 36 (1) (2016) 239–242, https://doi.org/10.1016/j.jeurceramsoc.2015.09.012.
[41] P. Zhang, S. Li, Z. Zhang, General relationship between strength and hardness, Mater. Sci. Eng., A 529 (2011) 62–73, https://doi.org/10.1016/j.msea.2011.08.061.
[42] M.F. Ashby, Materials Selection in Mechanical Design, Elsevier Science, 2017.
[43] A.A. Wereszczak, A.S. Barnes, K. Breder, S. Binapal, Probabilistic strength of 111 n-type silicon, J. Mater. Sci.: Mater. Electron. 11 (2000) 291–303, https://doi.org/10.1023/A:1008973231053.
[44] T. Liu, P. Ge, W. Bi, Y. Gao, The study of crack damage and fracture strength for single crystal silicon wafers sawn by fixed diamond wire, Mater. Sci. Semicond. Process. 134 (2021) 106017, https://doi.org/10.1016/j.mssp.2021.106017.
[45] R. Danzer, On the relationship between ceramic strength and the requirements for mechanical design, J. Eur. Ceram. Soc. 34 (15) (2014) 3435–3460, https://doi.org/10.1016/j.jeurceramsoc.2014.04.026.
[46] Y. Hirsh, S. Gorfman, D. Sherman, Cleavage and surface energies of $LiNbO_3$, Acta Mater. 193 (2020) 338–349, https://doi.org/10.1016/j.actamat.2020.03.046.
[47] S. Würzner, R. Buchwald, H.J. Möller, Surface damage and mechanical strength of silicon wafers, Phys. Stat. Solidi (c). 12 (2015) 1119–1122, https://doi.org/10.1002/pssc.201400227.
[48] G.D. Quinn, Fractography of Glasses and Ceramics, US Government Printing Office, Washington, 2007.
[49] N. Naumenko, Suppression of propagation losses in TC SAW resonators using thin plates of $LiTaO_3$ bonded to quartz substrates, in: 2018 IEEE International Ultrasonics Symposium (IUS), 2018, pp. 1–9, https://doi.org/10.1109/ULTSYM.2018.8579813.
[50] T. Takai, H. Iwamoto, Y. Takamine, H. Yamazaki, T. Fuyutsume, H. Kyoya, T. Nakao, H. Kando, M. Hiramoto, T. Toi, M. Koshino, N. Nakajima, High-performance SAW resonator on new multilayered substrate using $LiTaO_3$ crystal, IEEE Trans. Ultrason. Ferroelectr. Freq. Control 64 (9) (2017) 1382–1389, https://doi.org/10.1109/TUFFC.2017.2738119.